ISIJ International, Vol. 54 (2014), No. 12, pp. 2844–2853

Evolution of Microstructure and Texture during Isothermal Annealing of a Heavily Warm-rolled Duplex Steel

Mohammed ZAID AHMED and Pinaki Prasad BHATTACHARJEE*

Department of Materials Science and Metallurgical Engineering, Indian Institute of Technology Hyderabad, Ordnance Factory Estate, Yeddumailaram, 502205 AP India.

(*Received on April 14, 2014; accepted on July 28, 2014*)

The evolution of microstructure and texture during isothermal annealing of a heavily warm-rolled duplex steel (DSS) was studied. For this purpose a DSS steel was hot rolled, homogenized at 1 448 K and subsequently warm-rolled to 90% reduction in thickness at 698 K and 898 K. This was followed by isothermal annealing at 1 448 K for different time intervals up to 7 200 seconds. Lamellar microstructure with alternate arrangement of deformed ferrite and austenite bands was observed in the as warm-rolled condition. The ferrite in DSS warm-rolled at 698 K showed much stronger α-fiber (Rolling direction (RD)//<110>) than γ-fiber (Normal direction (ND)//<111>) as compared to the ferrite in DSS warm-rolled at 898 K. The austenite in warm-rolled DSS showed a predominantly pure metal (or copper type) texture. Upon annealing the lamellar morphology of the as warm-rolled structure transformed into a bamboo type morphology for short annealing time but finally broke down with increasing isothermal annealing time due to mutual interpenetration of the two phases. Retention of deformation texture components and presence of annealing twins in austenite indicated discontinuous recrystallization. Despite differences of texture in the as warm-rolled condition the ferrite in annealed DSS showed much stronger α-fiber as compared to γ-fiber due to strong recovery behavior of ferrite during annealing. The texture evolution in the two phases was not affected by the presence of the other phase while grain growth was significantly restricted due to the presence of the other phase.

KEY WORDS: duplex steels; warm-rolling; annealing; microstructure; texture; EBSD.

1. Introduction

The process of annealing in metallic materials following heavy deformation results in the development of microstructure and characteristic crystallographic texture which are crucial for achieving desired properties for different applications. Consequently, the evolution of microstructure and texture during recrystallization of deformed materials has been studied energetically in a wide variety of materials including pure metals, single phase and two-phase alloys, composites and intermetallics.[1] However, amongst the two-phase alloys the main focus has been on those materials having the second phase present as dispersed particles such as precipitation-hardening or age-hardening aluminum alloys. In contrast, the recrystallization behavior of another group of two-phase materials with duplex microstructure such as (α+β) brass or duplex stainless steels (DSS) where both the phases have a grain structure have been studied to a much lesser extent. Previous studies on duplex alloys summarized by Humphreys *et al.*[2] show that the recrystallization behavior of duplex alloys can be significantly affected by imposed strain, difference in homogenization and annealing temperature. Duplex alloys also show rather complex phase transformations and precipitation during recrystallization which can be helpful for processing materials having fine microstructure combined with other attractive mechanical properties.[2]

The motivation of the present work is to study the recrystallization behavior of duplex alloys from a fundamental point of view using heavily warm-rolled DSS with nearly equal volume fraction of ferrite and austenite as a model system. Warm-rolling of DSS is considered particularly important in the present work as additional complexities arising out of stress-induced martensitic transformation from austenite which can easily happen during cold-rolling is avoided. In addition, although thermo-mechanical processing involving cold-rolling and annealing of DSS has been reported,[3–8] the effect of warm-rolling on the evolution of microstructure and texture has been clarified only recently by the present authors.[9] The present investigation is aimed to clarify the evolution of microstructure and texture during subsequent annealing of a heavily warm-rolled DSS. This should be of interest for designing novel thermo-mechanical processing routes for DSS.

2. Experimental

2.1. Processing

An as-cast DSS ingot having the shape of a tapered cyl-

* Corresponding author: E-mail: pinakib@iith.ac.in
DOI: http://dx.doi.org/10.2355/isijinternational.54.2844

inder with top and bottom diameters of 72 mm and 62 mm, respectively and height of 290 mm was used in this work. The chemical composition of the DSS alloy is shown in **Table 1**. The as-cast ingot was subjected to a series of thermo-mechanical processing steps consisting of hot-forging or cogging at 1 473 K to a dimension of 60 mm (thickness) × 55 mm (width) × 300 mm (length) followed by reduction in thickness (~82.5%) by hot-rolling at 1 398 K to a final thickness of 10.5 mm. The total reduction during hot-rolling was achieved in seven passes. Rectangular samples having dimensions 30 mm (width) × 80 mm (length) were cut from the hot-rolled material and homogenization annealed at 1 398 K for 7 200 s in a tubular furnace in flowing argon atmosphere to yield nearly equal volume fraction of austenite and ferrite. The homogenized DSS was used as the starting material and subsequently warm-rolled up to ~90% reduction in thickness at two different temperatures, 698 K and 898 K using a laboratory scale rolling equipment (SPX Precision Equipment, USA). The thickness of the homogenized material (~10 mm) was reduced in steps of ~1 mm to a thickness of 2 mm (total 8 rolling passes). Beyond that, due to increased strain hardening the final thickness of 1 mm (corresponding to ~90% reduction in thickness) was achieved in steps of 0.5 mm using two additional passes. Thus, total thickness reduction was achieved in 10 passes. A box type furnace was used for the pre-heating purpose and isothermal holding time of 15 minutes was used before each warm-rolling pass to achieve homogeneity in temperature. The warm-rolling was carried out along the original direction of hot-rolling. In order to minimize the sudden quenching effect the rolls were pre-heated to 523 K during warm-rolling. The warm-rolled samples were immediately water quenched after every warm-rolling pass. The 90% warm-rolled samples were subsequently isothermally annealed in a conventional horizontal cylindrical furnace at 1 448 K for different time intervals up to 7 200 s in flowing argon atmosphere and immediately water-quenched following the heat-treatment.

A simple sample nomenclature (**Table 2**) is used for the different warm-rolled and annealed samples for ease of discussion. The two series of samples warm-rolled at temperatures 698 K and 898 K are designated as A and B, respectively. The added numbers are used to denote the isothermal holding-time in minutes (for *e.g.* 0 and 2 indicate the as warm-rolled and warm-rolled/annealed for 2 minutes condition, respectively). It may be noted that the annealing was carried out at the same temperature at which the samples were homogenized to avoid major effect of change in phase fraction during annealing.

Table 1. Chemical composition of the experimental DSS.

Element	C	S	Cr	Mn	Ni	P	Si	Mo	Fe
Weight%	0.08	0.001	24.18	0.14	10.5	0.017	0.45	3.11	balance

Table 2. Sample designation system used in the present work.

Warm-rolling temperature (K)	Sample designation				
	As warm-rolled (90%)	Isothermal holding time (minutes) during subsequent annealing at 1 448 K			
		2	20	30	120
698	A0	A2	A20	A30	A120
898	B0	B2	B20	B30	B120

2.2. Characterization

The microstructure and microtexture of the deformed materials were characterized using electron back scatter diffraction (EBSD) system (Oxford Instruments, UK) attached to a FEG-SEM (Make: Carl Zeiss, Germany, Model: SUPRA-40). Samples for EBSD investigation were prepared by careful mechanical polishing followed by electropolishing using a solution consisting of 700 ml ethanol, 120 ml distilled water, 100 ml glycerol, and 80 ml perchloric acid at room temperature. The EBSD data was acquired using a fine scan step size of 0.05 μm (50 nm) for deformed materials. For annealed materials the scan step size was decided such that at least 5 scan points were acquired from a single grain for achieving high reliability. The acquired EBSD dataset were analyzed using TSL-OIM^{TM} software. Several EBSD scans were acquired from each deformed and annealed samples. The acquired scans were merged to calculate the pole figures and the ODFs using the series expansion method with series rank (L) 22. Orientation data of at least 4000 grains were analyzed for each phase for statistical reliability. A cut-off angle of 15° was used for calculating the volume fraction of different texture components.

3. Results

3.1. Evolution of Microstructure and Texture during Warm-rolling

The phase map of the starting homogenization annealed material (**Fig. 1**(a)) shows nearly equal volume fraction of the two constituent phases. The microstructure shows somewhat elongated morphology of the two phases along the prior hot-rolling direction. The phase maps of the A0 (Fig. 1(b)) and B0 (Fig. 1(c)) show lamellar arrangement of alternative bands of deformed ferrite and austenite. The individual phase bands are further subdivided by HAGBs extended parallel to the phase boundaries and inside the phase bands LAGB network exists (not shown in the phase maps for clarity). The phase map of A0 specimen shows more fragmented regions and thick ferrite blocks as compared to very fine lamellar structure almost free of fragmentation in the B0 specimen.

The misorientation gradients along the arrow marks (misorientation between starting point or origin and any point along the arrow) inside the deformed ferrite bands of A0 and B0 are shown in **Fig. 2** which show low misorientation (<15°) build up inside the ferrite bands.

Figure 3 compares the φ_2=45° section of the ODF of ferrite in homogenized (Fig. 3(a)), A0 (Fig. 3(b)) and B0 (Fig. 3(c)) specimens. Figure 3(d) shows the ideal locations of the components along the two well-known texture fibers in bcc materials for ease of comparison. The φ_2=45° section of the ODF of ferrite of homogenized material (Fig. 3(a)) does not show strong γ (ND//<111>) fiber but indicates the presence of a strong {111}<121> orientation as a single component only. Noticeable presence of the rotated cube component ({001}<410>) shifted along the φ_1 axis by ∓ 15° is evidenced. The φ_2=45° section of the ODF of ferrite in A0 (Fig.

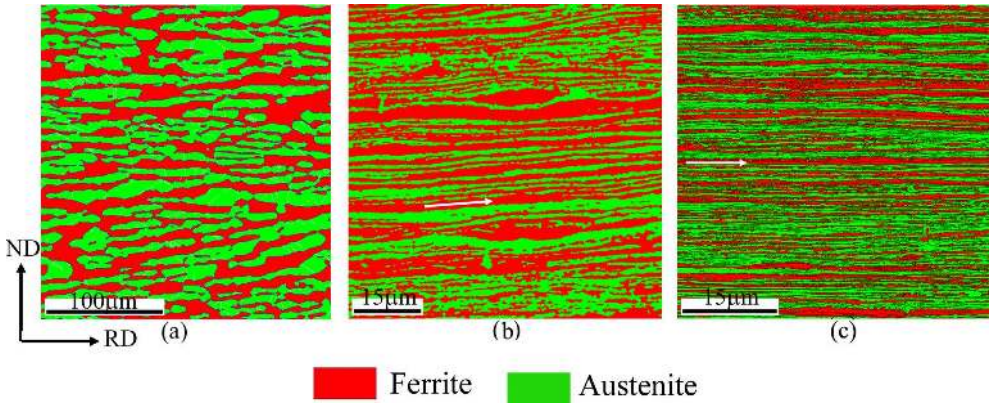

Fig. 1. Phase maps of (a) homogenized, (b) A0 and (c) B0 specimens. (Online version in color.)

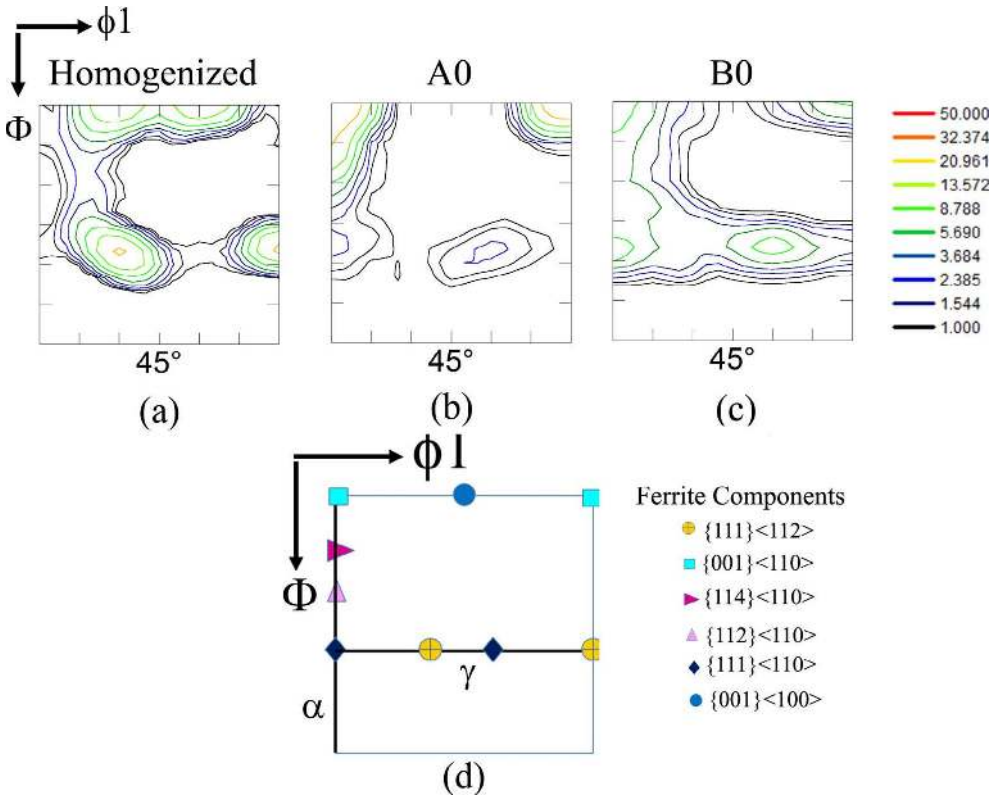

Fig. 3. φ_2=45° section of the ODFs of ferrite in (a) homogenized, (b) A0, (c) B0 specimens; (d) shows the location of ideal components in the ODF section. (Online version in color.)

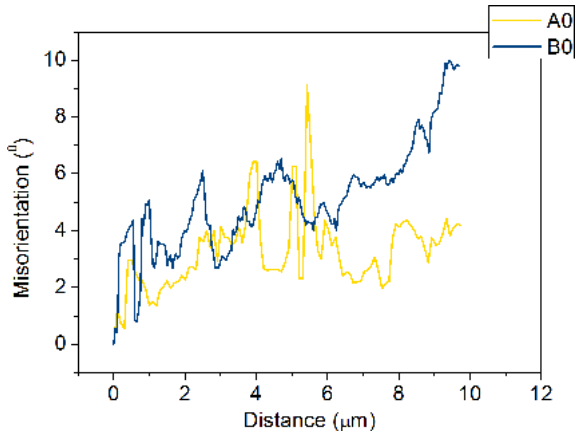

Fig. 2. Point to origin misorientation gradient along the arrows inside ferrite bands in Figs. 1(b) and 1(c). (Online version in color.)

3(b)) does not show the presence of the γ-fiber but shows strong {001}<110> component of the α-fiber. Minor presence of the {111}<110> component which is located at the intersection of the α and γ fibers is also noticed. In sharp contrast to the texture of ferrite in A0 specimen, the φ_2=45° section of the ODF of ferrite in B0 (Fig. 3(c)) shows strong presence of both α and γ fibers.

Figure 4 shows the φ_2=0°, 45° and 65° sections of the ODF of austenite of the starting homogenized DSS (Figs. 4(a)–4(c)) and those of the A0 (Figs. 4(d)–4(f)) and B0 (Figs. 4(g)–4(i)). Ideal locations of typical FCC rolling texture components, such as, S ({123}<634>), copper (or Cu) ({112}<111>), brass (or B_S) ({110}<112>), Goss (or G) ({011}<100>) and the cube (or C) component ({001}<100>) are indicated in the ODF sections. The ODF sections of the homogenized starting material (Figs. 4(a)–4(c)) clearly shows rather weak texture of austenite. The ODF sections

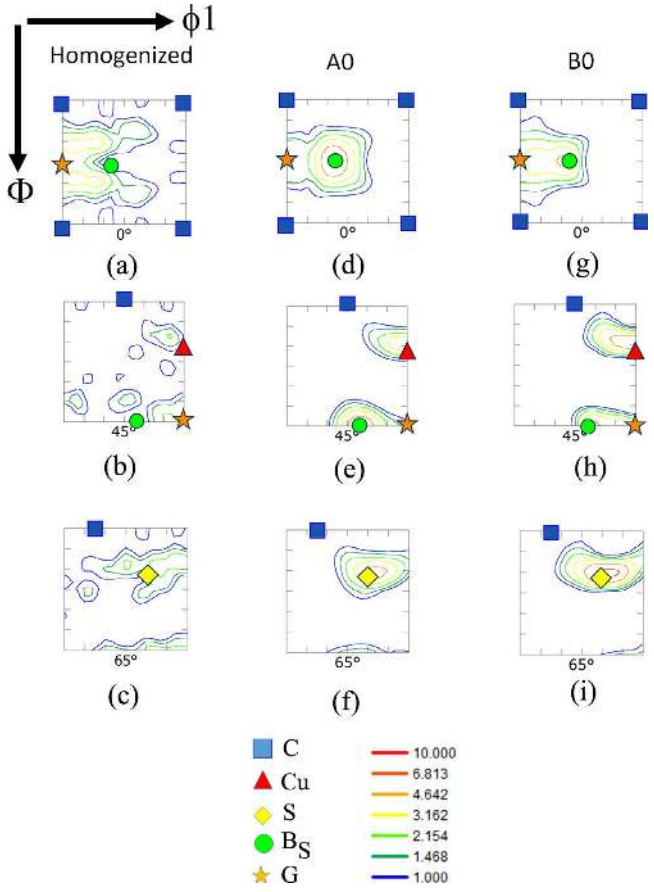

Fig. 4. φ_2=0°, 45° and 65° sections of the ODFs of austenite in (a) homogenized, (b) A0 and (b) B0 specimens. (Online version in color.)

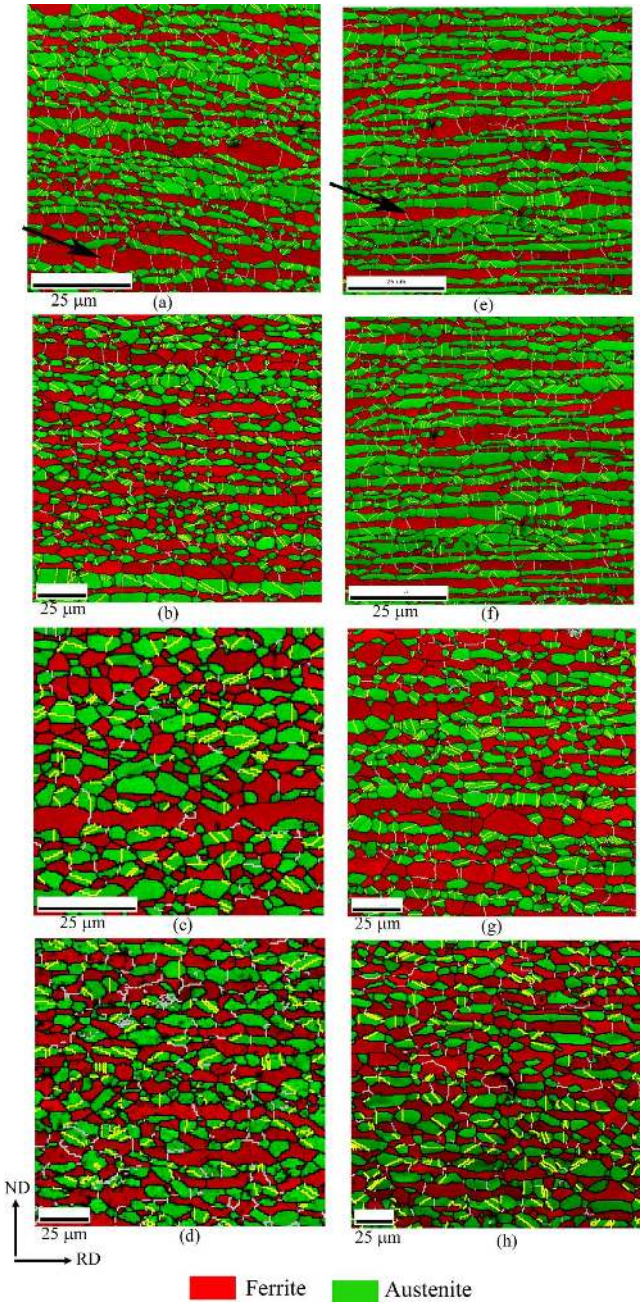

Fig. 5. Phase maps of (a) A2, (b) A20, (c) A30 (d) A120, (e) B2, (f) B20, (g) B30 and (h) B120. (Online version in color.)

of both A0 and B0 specimens show strengthening of the characteristic pure metal type texture components, namely, S, Cu and the B_S following warm-rolling. However, the intensity distribution in the ODF sections of the A0 specimen indicates that strength of the B_S component is comparable to that of the S component (~17%) but more than the Cu component (9%). In contrast, the B0 specimen shows stronger S component (~22%) as compared to the B_S (~11%) and Cu (~12%) components. Thus, while the texture of austenite of both A0 and B0 specimens may be characterized as pure metal type, this is evidently more pronounced in the B0 specimen.

3.2. Evolution of Microstructure during Annealing

Figure 5 shows the evolution of microstructure during isothermal annealing at 1 448 K of different warm-rolled samples. After annealing for 120 s (2 mins) the lamellar morphology of the warm-rolled materials (Figs. 1(b) and 1(c)) is still evidenced by the extended phase bands along the RD (marked by arrows) in the phase maps of A2 (Fig. 5(a)) and B2 (Fig. 5(e)). However, at the same time the continuity of the phase bands appears to be broken locally. The phase bands of the two constituent phases do not reveal LAGB network as is observed in the microstructures of the as warm-rolled materials.[10] Instead, the phase bands mostly show grain boundaries normal to the phase boundaries resulting in a bamboo type morphology. In case of ferrite the perpendicular phase boundaries are frequently LAGBs while in austenite those are mostly HAGBs. Profuse annealing twins are clearly observed inside the austenite bands (annealing twin boundaries are revealed by yellow lines). Each individual phase band is one grain thick when measured along the ND.

The lamellar phase bands continues to break down with increasing annealing time. This is evidenced by the appearance of regions with comparatively more globular morphology in the microstructures of the specimens annealed for 1 200 s (20 minutes) as shown in the phase maps of A20 (Fig. 5(b)) and B20 (Fig. 5(f)). Annealing for 1 800 s (30 minutes) results in extensive break-down of the lamellar phase bands concurrent with the distribution of the two-phases throughout the microstructure. Such regions are quite evident in the microstructure of the A30 (Fig. 5(c)) and B30 (Fig. 5(g)) specimens. Further annealing even for 7 200 s

(2 hours) does not change the morphology significantly (Figs. 5(d) and 5(h)).

Figure 6 summarizes the evolution of key structural parameters of the two constituent phases in different warm-rolled materials during annealing. The ferrite phase fraction plot (Fig. 6(a)) shows that the ferrite phase fraction decreases initially for shorter isothermal holding times as compared to the fraction in the as warm-rolled condition. However, the ferrite fraction increases with increasing annealing time and approaches a stable value of ~0.50 observed in the homogenized starting material after 1 200 s (20 minutes) annealing. Figures 6(b) and 6(c) show the variation of ferrite and austenite grain thickness (measured along the ND), respectively with annealing time. Since each phase band is mostly one grain thick as observed from the microstructures already (Fig. 5), the grain thickness is thus same as the phase thickness for the different annealed materials. Both the ferrite and austenite grain thickness increase with increasing time but extensive coarsening of the microstructure is not observed even after annealing for 7 200 s (2 hours), which is demonstrated by quite similar recrystallized grain thickness along ND of ~5–6 μm for the two phases.

The aspect ratio (defined by ratio of thickness along the ND divided by length along RD) of ferrite (Fig. 6(d)) is low (~0.34–0.35) in different warm-rolled materials after annealing for 120 s (2 minutes) but increases with increasing annealing time up to 1 800 s (30 minutes). The aspect ratio does not show any perceptible change for further isothermal holding. However, the aspect ratio of ferrite in the annealed B series specimens shows somewhat lower average value for longer annealing time (> 1 800 s (30 minutes) isothermal holding time) as compared to that in the annealed A series specimens which is evident from the aspect ratio of ferrite in the B120 specimen of ~0.40 as compared to that in the A120 specimen (~0.45).

The aspect ratio of austenite (Fig. 6(e)) shows very similar trend observed in ferrite; increasing with increasing isothermal holding time but no significant change beyond isothermal holding time of 1 800 s (30 minutes). The aspect ratio of austenite is found to be evidently larger than ferrite in the same warm-rolled condition. Further the aspect ratio of austenite in the annealed B series specimens is found to be lower as compared to that in the annealed A series specimens. It might be noted that the variation in the aspect ratio is quite consistent with the microstructural observation of breakdown of elongated lamellar structure *i.e.* decrease of length along RD with increasing isothermal holding time. It may be noted that increase in fractional aspect ratio towards a value of unity also indicates tendency towards development of a more globular morphology.

3.3. Evolution of Texture during Annealing

Figure 7 shows the φ_2=45° sections of the ODFs of ferrite in A and B series DSS specimens in different isothermally annealed conditions. The ODF sections of the annealed A series specimens (Figs. 7(a)–7(d)) clearly reveal the presence of much stronger α fiber as compared to the γ-fiber (The ODF section showing the ideal locations of different components in Fig. 3(d) is referred to for clear understanding). In the A2 specimen (Fig. 7(a)) presence of the α fiber components {112}<110> is noticed along with the {001}<110> component. The {001}<110> component is strengthened while the {112}<110> component is significantly weakened with increasing isothermal holding time. The intensity distribution along the γ fiber remains weak throughout the annealing process. The intensity along the γ fiber in the A2 specimen is found closer to the {111}<112> location (volume fraction ~14%) but slightly higher intensi-

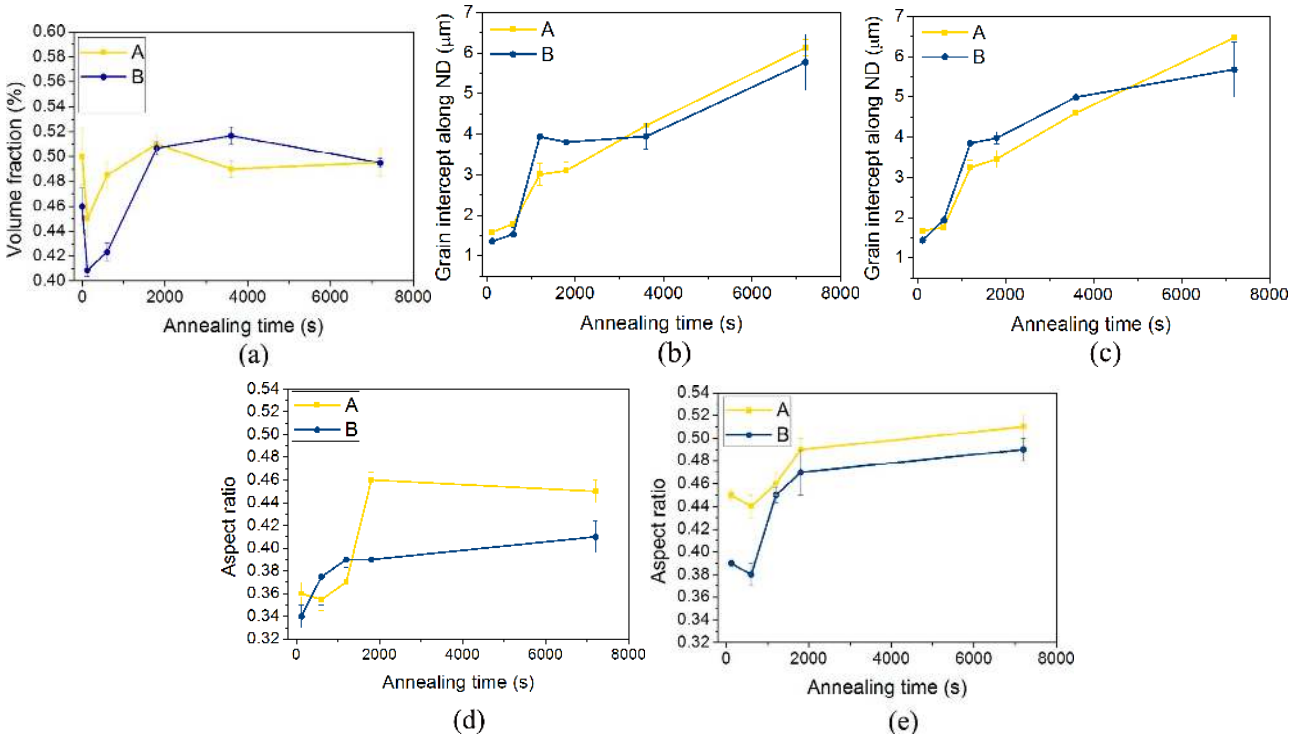

Fig. 6. Change in (a) ferrite phase fraction, (b) ferrite and (c) austenite grain intercept along the ND, (d) ferrite and (e) austenite aspect ratio with isothermal annealing time. (Online version in color.)

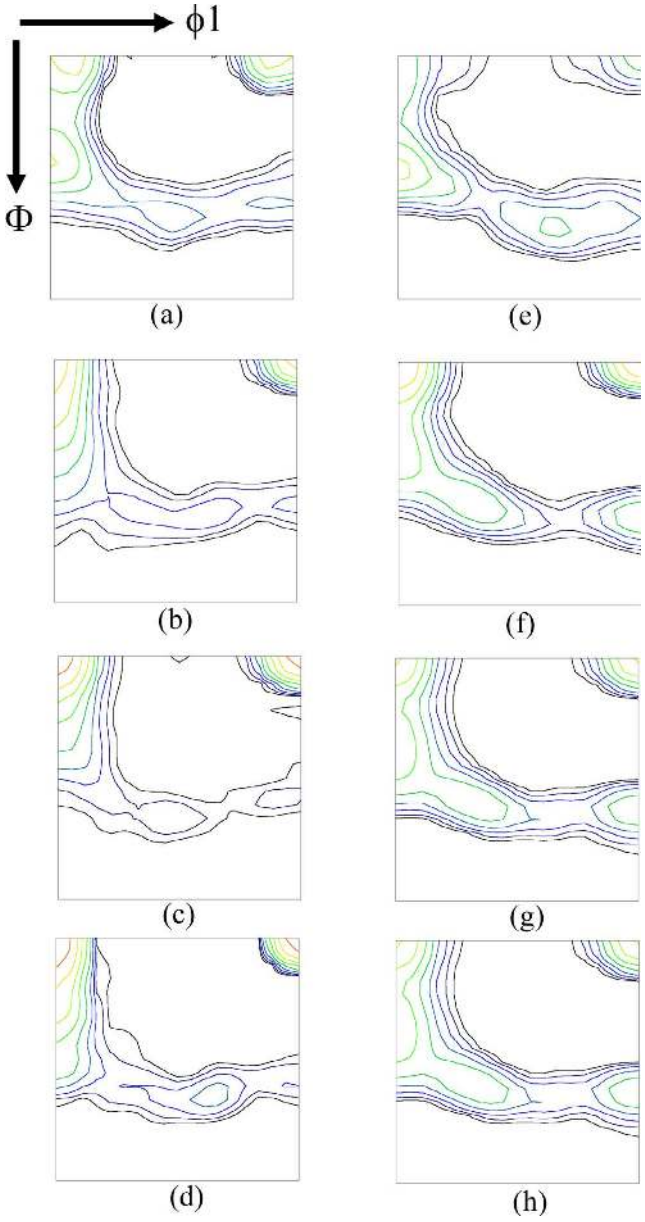

Fig. 7. φ_2=45° section of the ODF of ferrite in (a) A2, (b) A20, (c) A30, (d) A120, (e) B2, (f) B20, (g) B30 and (h) B120. Intensities of the contour lines are same as in Fig. 3. (Online version in color.)

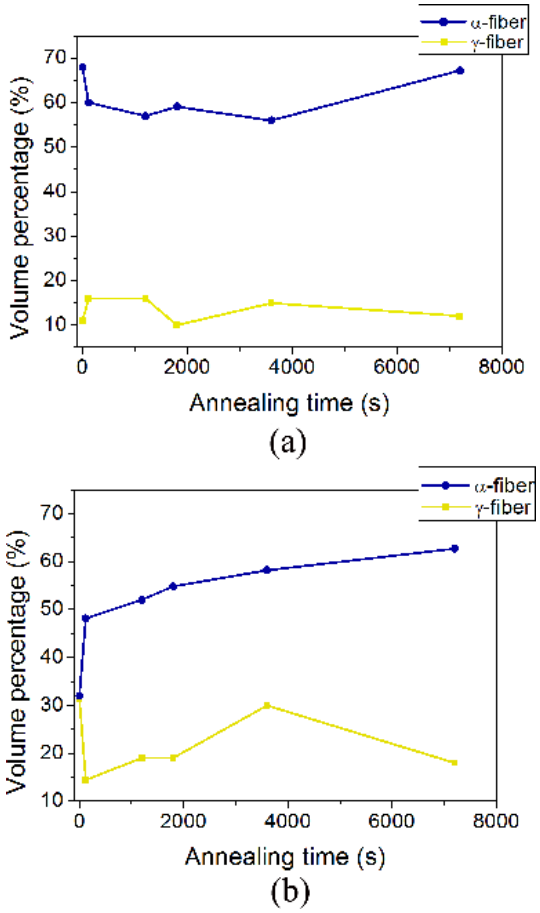

Fig. 8. Evolution of α and γ fiber fraction with isothermal holding time in ferrite in (a) A and (b) B series specimens. (Online version in color.)

ty is observed for {111}<011> (volume fraction ~7.6%) as compared to {111}<112> (volume fraction ~6.0%) in the A120 specimen.

The evolution of the two prominent texture fibers during isothermal annealing of the A series specimens is shown quantitatively in **Fig. 8**(a). The volume fraction of the α and γ fibers in the A0 specimen is ~67% and 11%, respectively while in the A2 specimen the volume fraction of the two fibers are ~60% and 16%, respectively indicating only minor changes in the volume fraction of the two fiber components after complete recrystallization. The volume fraction of the two fibers does not show any significant change even after isothermal annealing for 7 200 s (2 hours) so that the volume fractions of the α and γ fibers in the A120 specimen is found to be ~67% and 12%, respectively. Thus, the annealing textures of the A series specimens are evidently similar to the texture in as warm-rolled condition.

The φ_2=45° sections of the ODFs of ferrite (Figs. 7(e)–7(h)) in different isothermally annealed B series specimens also show the presence of both α and γ fiber components (The ODF section showing the ideal locations of different components in Fig. 3(d) is referred to for clear understanding). The intensity distribution of the contour lines clearly show the presence of much stronger α fiber as compared to the γ fiber after different annealing treatments despite the fact that in the as warm-rolled material (*i.e.* in B0 specimen) the α and γ fibers show comparable strength with volume fraction of ~32%. This is easily understood from the quantitative evolution of the two fibers with annealing time (Fig. 8(b)). The α fiber shows significant increase to 48% after annealing for 120 s (2 minutes) while the fraction of the γ fiber decreases to 15%. The strength of the α fiber remains decidedly much higher than the γ fiber in different isothermally treated specimens. In contrast to the A2 specimen, the main intensity peak along the γ fiber in the B2 specimen is located close to the {111}<110> location which shows higher volume fraction (~15%) than {111}<112> (~10%) but is weakened with increasing annealing time and intensity peak shifts closer to the {111}<112> location. In the B2 specimen slightly higher intensity along the α fiber is observed at the {112}<110> location than the {001}<110>. This is consistent with higher volume fraction of the {112}<110> component (~27%) as compared to the {001}<110> component (~20%) in the B2 specimen. The {001}<110> component is

strengthened with isothermal holding time very similar to the behavior observed in case of the A series specimens.

Figure 9 shows φ_2=0°, 45° and 65° sections of the ODFs of austenite in different isothermally annealed A and B series DSS specimens. The ODF sections of both the annealed A series (Fig. 9(a)) and B series (Fig. 9(b)) specimens after different annealing treatments clearly indicate the retention of pure metal type texture after annealing. The intensity distribution in the ODF section of annealed A series specimen shows stronger S and B_S components as compared to the Cu component particularly after longer isothermal holding time. On the other hand, the intensity distribution in the ODF sections of annealed B series specimen suggests presence of B_S and Cu components having similar strength.

Figure 10 shows the volume fraction of different texture components in the isothermally annealed A (Fig. 10(a)) and B (Fig. 10(b)) series specimens. Importantly, the typical brass recrystallization texture component (BR) {236}<385> which is often described as the major recrystallization texture component in low stacking fault energy materials[2] is evidently not the strongest component. It is clearly observed that in the two DSS series of samples the volume fraction of the S component decreases after 120 s (2 minutes) isothermal annealing as compared to the as warm-rolled condition. However, the S component remains as the most prominent texture component and appears particularly strong in specimens isothermally annealed for longer durations. The S component shows very similar volume fraction ~21% and 23% in the A120 and B120 samples, respectively.

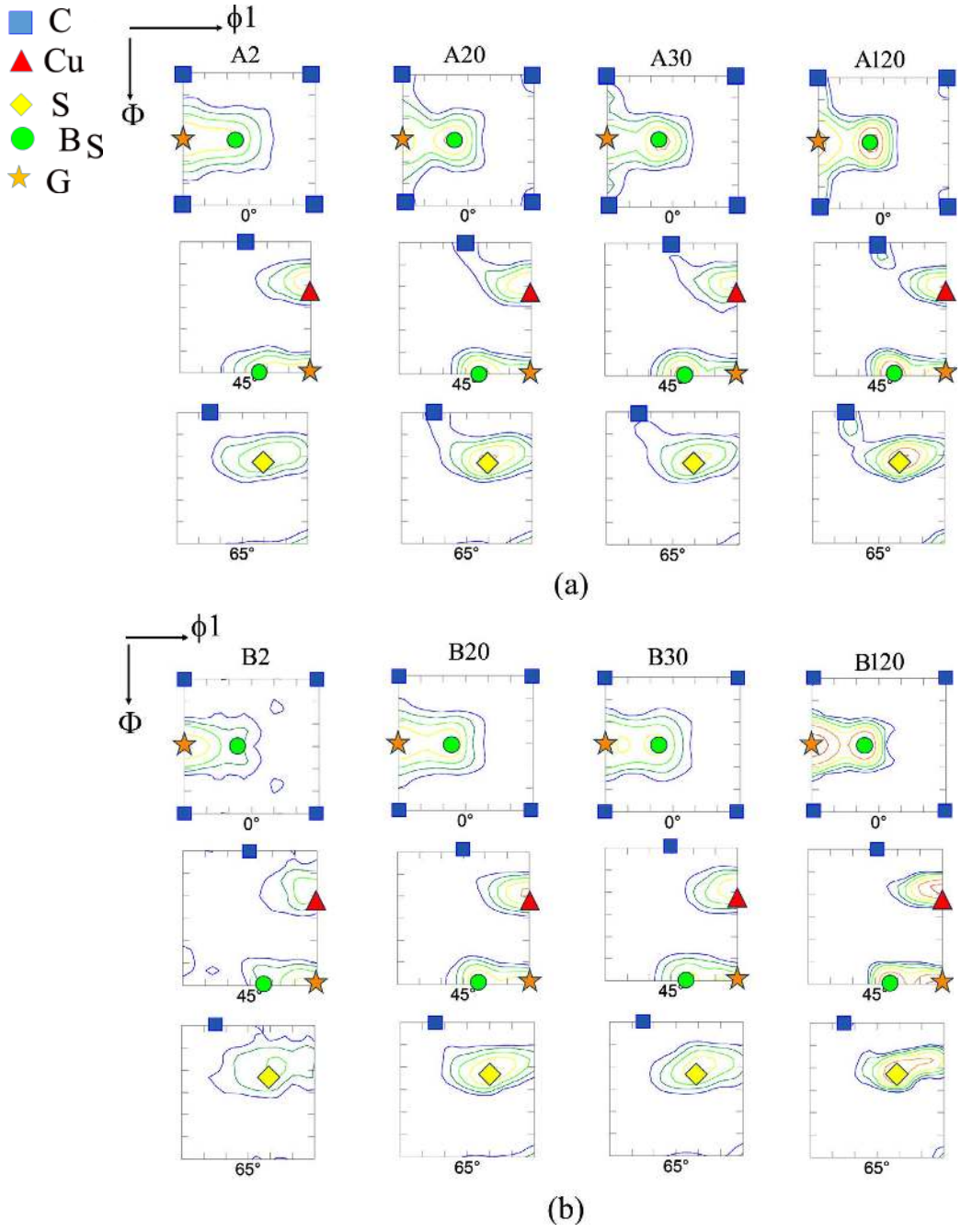

Fig. 9. φ_2=0°, 45° and 65° sections of the ODFs of austenite in isothermally annealed A and B series DSS specimens. Intensities of the contour lines are same as in Fig. 4. (Online version in color.)

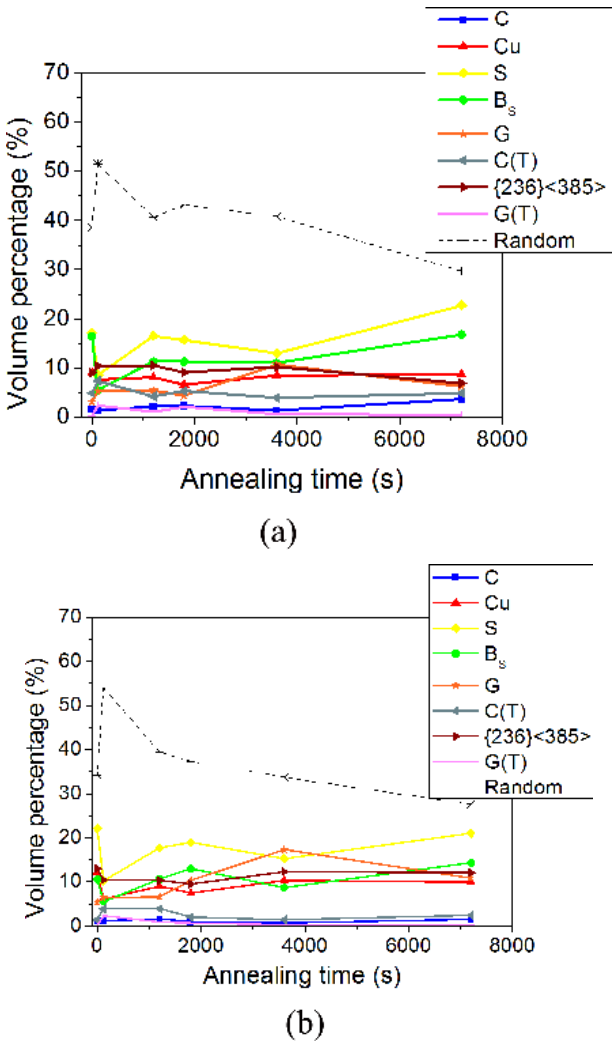

Fig. 10. Evolution of texture components with annealing time in austenite in (a) A and (b) B series of DSS. C(T) and G(T) are the twin orientations of C and G orientations, respectively. (Online version in color.)

B_S, Cu and G components are also observed in different annealed specimens amply corroborating qualitative assessment of presence of pure metal type texture deduced from the ODF analysis. In good agreement with ODF analysis it is further observed that the B_S component is stronger than the Cu component in the annealed A series specimens for longer annealing times while the volume fractions of the two components are rather similar in the annealed B series specimens. However, the twin component of the G (denoted by G(T)) {11 11 8}<4 4 11> shows negligible presence in both the annealed A and B series specimens having volume fraction usually less than 1%. The volume fraction of the random components increase initially after 120 s (2 minutes) annealing as compared to the as warm-rolled materials but decreases with increasing annealing time indicating progressive strengthening of the annealing texture.

4. Discussion

4.1. Evolution of Microstructure and Texture during Warm-rolling

As already observed from Fig. 1, warm-rolling has significant impact on the microstructure and texture formation in DSS. This is evidenced by the fragmented microstructure in the A0 sample and a rather strong α fiber in the ferrite phase as compared to the B0 specimen. The reasons for these observations have recently been clarified by the phenomenon of interaction of carbon atoms with dislocations.[10] Since the warm-rolling temperature of 698 K is well within the reported dynamic strain aging regime of DSS alloys[11] carbon atoms can readily lock the dislocations resulting in increased flow stress, suppression of grain sub-division and mechanical fragmentation of grains which are consistent with the fragmented microstructure present in the A0 specimen (Fig. 1(b)). Further, the dynamic strain aging also results in the preferential retardation of slip on the {110}<111> system[12] resulting in the strengthening of the α fiber components at the expense of the γ fiber components[13] which is clearly evidenced in the texture of ferrite in A0 specimen (Fig. 3). At the warm-rolling temperature of 898 K the mobility of the carbon atoms is high so that microstructure and texture formation remains largely unaffected. This results in the presence of both γ and α fibers in the B0 specimen. It might be noted that hot-rolled and homogenized specimen does not exhibit γ-fiber but a strong {111}<112> orientation as the main texture component (Fig. 3(a)). Development of γ fiber from strong {111}<112> orientation is evident during warm-rolling. Strengthening of the α-fiber happens beyond 70% deformation during warm-rolling. However, the strength of the α fiber is affected by carbon locking of dislocations as already explained so that the texture of ferrite in DSS warm-rolled at two different temperatures shows remarkable difference. Thus, while the strength of the two texture fibers in steels is known to be greatly affected by deformation,[14] in the present case the texture development is also greatly affected by the temperature of warm-rolling.

The austenite shows a pure metal texture at the two warm-rolling temperatures. This is attributed to the increasing SFE with increasing temperature of warm-rolling so that preference for the formation of deformation twinning is reduced in favor of dislocation slip.[10] The stronger B_S component observed in the A0 specimen (*i.e.* at the lower temperature of warm-rolling) as compared to that in the B0 specimen (*i.e.* at the higher temperature of warm-rolling) (Fig. 4) is in good agreement with the mechanism suggested.

4.2. Evolution of Microstructure during Recrystallization

It has been observed from Fig. 6(a) that in both series of DSS the ferrite phase fraction decreases initially after annealing for 120 s (2 minutes) but recovers to the value observed in as homogenized condition during longer period of annealing. Since the annealing has been carried out in a conventional furnace ferrite to austenite conversion happens before the material is heated up to the annealing temperature 1 448 K. For shorter annealing duration the phase equilibrium could not be achieved. However, for longer duration the phase equilibrium between ferrite and austenite is re-established and volume fraction ratio of 50:50 (same as that in the as-homogenized material) is obtained.

The major point of interest in the present study, however, is the evolution of microstructure during recrystallization.

The microstructural observations (Fig. 5) and aspect ratio variation (Figs. 6(d) and 6(e)) of the two warm-rolled DSS alloys clearly indicate the gradual transformation of a bamboo type lamellar morphology towards a comparatively more globular morphology with increasing isothermal annealing time. This structural evolution is indicative of the recovery in the ferrite phase which is also observed during annealing of cold rolled DSS alloys.[3] In the as warm-rolled condition ferrite already has a more recovered microstructure[9] so that driving force for recrystallization is low. The sub-grains bounded by LAGBs thus grow during subsequent annealing. Due to the lamellar morphology of the two phases extensive lateral growth along the RD direction is favored even after the ferrite grains grow along the ND to the full thickness of the phase bands. This results in lower aspect ratio of the ferrite grains after short isothermal holding time. Meanwhile the lateral growth of the sub-grains and low misorientation build-up inside the ferrite bands (Fig. 2) ensure that neighboring sub-grains inside ferrite phase bands are separated by LAGBs resulting in the well-developed bamboo type morphology observed in the ferrite after short isothermal holding time. In case of the bamboo type austenite morphology the perpendicular grain boundaries are mostly HAGBs. The austenite also shows higher aspect ratio as compared to the ferrite in the same isothermally annealed condition. These microstructural observations indicate that the primary softening mechanism in austenite is discontinuous recrystallization due to which recrystallized grains bounded by HAGBs with comparatively more globular morphology *i.e.* higher aspect ratio (as compared to the ferrite grains) form inside the austenite phase bands. The recrystallized austenite grains grow to extend over the full thickness of the austenite bands very similar to the situation observed in case of ferrite. The lateral growth along the RD ensures that neighboring austenite grains are separated by HAGBs resulting in the characteristic bamboo morphology where the HAGBs run perpendicular to the phase boundaries. The evolution of texture in the two phases to be discussed shortly strongly supports the proposed softening mechanisms in the two constituent phases.

Annealing beyond 1 200 s (20 minutes) results in the gradual break down of the lamellar bamboo morphology and concurrent evolution of a comparatively more globular morphology. However, extensive microstructural coarsening is not observed even for long isothermal holding annealing (Figs. 6(b) and 6(c)). These microstructural observations are consistent with perceptible increase in the aspect ratio of both ferrite and austenite after annealing for 1 200 s (20 minutes) but no significant change for longer holding times. The suppression of grain growth could be attributed to hindrance to grain growth exerted by one phase on the other.

The break-down of the lamellar structure into comparatively more globular structure with increasing annealing time has also been reported in heavily cold-rolled and annealed DSS.[3] The structural adjustment is preceded by the break-down of the bamboo morphology initiated by mutual inter-penetration of the phases along the triple points consisting of two phase boundaries and one grain boundary. The pattern of microstructural evolution during annealing of the two warm-rolled DSS series specimens strongly suggests very similar mechanism as observed during annealing of cold rolled DSS.[3] However, the evolution of the microstructure is faster in the A series specimens, which is evidence by the higher aspect ratio of ferrite in the A30 specimen as compared to that of ferrite in the B30 specimen (Fig. 6(d)). This difference appears to be due to the more fragmented microstructure of the DSS warm-rolled at 698 K (Fig. 1(b)).

4.3. Evolution of Recrystallization Texture

The evolution of the recrystallization texture in the ferrite is affected by the characteristic softening by recovery already described before. Recovery preserves the characteristics of the deformation texture since nucleation of strain free grains typical during discontinuous recrystallization is absent. The two fiber components also behave differently in single phase ferrite during annealing owing to the orientation dependent stored energy.[2] The α fiber components such as the {001}<110> and {112}<110> would preferentially undergo recovery while the γ fiber components {111}<110> and {111}<112> due to their higher stored energy tend to show a recrystallization type behavior during annealing.[3,10] Thus depending on which softening mechanism is predominant strong α or γ fiber components will be developed in the annealing texture of ferrite.

It has already been discussed that ferrite in DSS warm-rolled at two different temperatures show markedly different textures. The ferrite in A0 shows much higher fraction of the α fiber components than γ fiber components in sharp contrast to rather comparable strength of the two fibers in ferrite of B0 specimen. Despite this apparent differences in the texture of ferrite in as warm-rolled conditions (*i.e.* in A0 and B0 specimens) the recrystallization texture of both A and B series specimens show much stronger α fiber than γ fiber though relative shift in the peak intensity along the two fibers is observed which however does not affect the total volume fraction of the two fibers significantly. This further indicates the dominant role of recovery on the development of annealing texture in ferrite of DSS. It might be noted that recovery of ferrite in cold-rolled and annealed DSS also leads to much stronger α fiber than γ fiber texture.[3] Processing by warm-rolling ensures dynamic recovery[9] and decrease the driving force for recrystallization which is conducive for suppressing recrystallization and strengthening the α fiber components.

The austenite of cold rolled and annealed DSS shows retention of deformation texture components particularly the G and the G(T) components.[3] However, the BR component which is often reported as a major texture component in the recrystallization texture of heavily deformed low SFE materials owing to the nucleation of this component in shear bands and subsequent growth selection of these grains due to the 40°<111> relationship with the B_S[15] is rather weak. The austenite in cold-rolled and annealed DSS does not develop strong BR component which is attributed to the absence of shear bands in the deformed matrix.[3]

The austenite of warm-rolled DSS alloys also retains the basic characteristics of the deformation texture during annealing *i.e.* typical pure metal type texture. These observations are similar to those reported in austenite in cold-rolled and annealed DSS.[3] This indicates very similar

recrystallization mechanism *i.e.* nucleation of grains (discontinuous recrystallization) with orientations pre-existing in the as deformed matrix but no preferential orientation selection. Discontinuous recrystallization and growth are also supported by presence of annealing twins in austenite. Nucleation from pre-existing orientations in deformed matrix but no preferential orientation selection will result in a situation where the annealing texture should be a random sampling of the deformation texture. Thus, observed differences in the texture of austenite should originate from the differences in texture of as warm-rolled materials *i.e.* of A0 and B0 specimens. This explains stronger S and B_S components than Cu component observed in annealed A series specimens as opposed to stronger S but B_S and Cu components of similar strength in annealed B series specimens. However, unlike austenite in cold-rolled and annealed DSS the G and G(T) components are not the major components. Since the fraction of G component is low in deformation texture, upon annealing the fraction of both G and G(T) remains low unlike the cold-rolled and annealed DSS.[3] In the present case a plausible explanation for the absence of the BR component appears to be the presence of a pure metal type texture instead of a dominant brass or alloy type texture in the warm-rolled conditions. Since Brass is not the dominant component of the warm-rolled texture the preferential growth advantage of BR grains would be greatly reduced preventing it from becoming the dominant texture component in the recrystallization texture.

5. Conclusions

(i) The lamellar morphology of the as warm-rolled structure transforms into a bamboo type morphology for short annealing time but finally breaks-down due to interpenetration of phases resulting in a comparatively more globular morphology with increasing isothermal holding time. The two phases behave differently during annealing. Ferrite shows recovery whereas austenite undergoes discontinuous recrystallization.

(ii) Much stronger α fiber as compared to γ fiber is observed in the two series of DSS steels during isothermal annealing although the strength of the α fiber in the as warm-rolled conditions are different. This is attributed to the recovery in ferrite due to the fact that α fiber components preferentially strengthen in contrast to γ fiber components.

(iii) Austenite retains the characteristics of the deformation texture after different isothermal annealing. This reveals that recrystallized grains originate from the orientations present in the deformed matrix but no preferential orientation selection.

(iv) The recrystallization texture of the two phases is not affected by the presence of the other phases, however, the grain growth is suppressed due to the hindrance to grain growth exerted by one phase on the other.

(v) Warm-rolling temperature affects the deformation microstructure and texture greatly, however, DSS warm-rolled at different temperatures show similar pattern of microstructure and texture evolution.

Acknowledgement

The authors would like to gratefully acknowledge Dr. G. Malakondaiah, former Director, DMRL, Hyderabad for his kind permission to prepare the starting alloy used in the present research work using the facilities at DMRL, Hyderabad and Dr. Raghu and Mr. Satheesh, scientists at DMRL, Hyderabad for their kind support in preparing the experimental alloy.

REFERENCES

1) R. D. Doherty, D. A. Hughes, F. J. Humphreys, J. J. Jonas, D. Juul Jensen, M. E. Kassner, W. E. King, T. R. McNelley, H. J. McQueen and A. D. Rollett: *Mater. Sci. Eng. A*, **238** (1997), 219.
2) F. J. Humphreys and M. Hatherly: Recrystallization and Related Annealing Phenomena, Elsevier, Amsterdam, (2004), 379.
3) J. Keichel, J. Foct and G. Gottstein: *ISIJ Int.*, **43** (2003), 1788.
4) W. Reick, M. Pohl and A. F. Padilha: *ISIJ Int.*, **38** (1998), 567.
5) T. Sahraoui, M. Hadji and M. Yahi: *Mater. Sci. Eng. A*, **523** (2009), 271.
6) T. Maki, T. Furuhara and K. Tsuzaki: *ISIJ Int.*, **41** (2001), 571.
7) J. Keichel, J. Foct and G. Gottstein: *ISIJ Int.*, **43** (2003), 1781.
8) J. Keichel, G. Gottstein and J. Foct: *Mater. Sci. Forum*, **318** (1999), 785.
9) P. P. Bhattacharjee, M. Zaid, G. D. Sathiaraj and B. Bhadak: *Metall. Mater. Trans. A*, **45** (2014), 2180.
10) I. Samajdar, B. Verlinden, P. Van Houtte and D. Vanderschueren: *Mater. Sci. Eng. A*, **238** (1997), 343.
11) R. Kolmorgen and H. Biermann: *Int. J. Fatigue*, **37** (2012), 86.
12) T. Senuma, H. Yada, R. Shimizu and J. Harase: *Acta Metall. Mater.*, **38** (1990), 2673.
13) J. L. Raphanel and P. Van Houtte: *Acta Metall.*, **33** (1985), 1481.
14) M. Z. Quadir, Y. Y. Tse, K. T. Lam and B. J. Duggan: *Mater. Sci. Forum*, **467–470** (2004), 311.
15) P. A. Beck: *Trans. Metall. Soc., AIME*, **194** (1952), 183.